CHAPTER 4

PREPARATION AND CHARACTERIZATION OF AERODYNAMICALLY LIGHT AND LARGE PARTICLES

4.1 INTRODUCTION

The success of a dry powder inhalation product is based on the ease of the powder dispersibility, which is mainly determined by the efficiency of the inhalation devices and by the physical properties of the powder. Many physical characteristics affect the dispersibility of the powder, including the nature of the material, particle size/distribution, particle shape/morphology, and moisture content. All these properties affect the interparticle (cohesion) forces and/or the particle-surface (adhesion) forces. Increased interparticle cohesion reduces powder segregation, resulting in aggregated particles that may not enter the deep lung. Increased particle surface adhesion decreases powder flowability and increases powder retention on all contact surfaces. However, even when particles are physically small enough (< 5μm), they are likely to be deposited on the wall of the respiratory tract on their way down to the alveolar regions of the lungs because inertial deposition is often the most dominating deposition mechanism. Particles with sufficient inertia can easily escape from streamlines of air flow and deposit on the airways. Based on the fluid dynamics, the aerodynamic diameter (D_a) of a particle (physical diameter D_s and density ρ_s) can be defined as $D_a = D_s \rho_s^{0.5}$ The significance of aerodynamic particle size lies in combining the influence of the particle's physical size and inertia. Assuming a light (low density) particle having the same physical size (D_s) as a heavy (high density) particle, the light particle will have a smaller aerodynamic size, i.e more aerodynamically favorable, than the heavy particle; therefore light particles are more likely to travel with air stream lines and reach in the deep lung for effective deposition. Changes in aerodynamic size for the particles of the same composition and shape can be made by changing the particle density. This concept has been addressed by Edward's et al using a different technique for preparing large porous particles (Edwards et al, 1997). In the present study, preparation of light and large particles by spray drying and freeze drying technique are being investigated. We will examine physical and aerosol properties of powders prepared by these two methods. Powder with superior aerosol performance will be further optimized statistically to establish the quantitative aspects of the effects and relationships among various formulation components of these high therapeutics payload large respirable powders.

4.2 MATERIALS

TB, AMK and L-leucine were received as a gift from Sun Pharma Advanced Research Centre, and Alembic limited (Vadodara, India) respectively. HSPC, Poloxamer 188 were obtained from Lipoid (Lipoid GmBH, Ludwigshafen, Germany) and BASF (Ludwigshafen, Germany) respectively. Coumarin was received as gift sample from Neelikon dyes (Mumbai, India).

4.3 PREPARATION OF AERODYNAMICALLY LIGHT AND LARGE PARTICLES

ALLP of AMK and TB was prepared by both spray and freeze drying process with varied proportion of drug (30-50% w/w) in the formulation. Spray and freeze drying parameters were previously optimized and the same operational parameters were used to prepare ALLP. Spray drying process parameters, such as feed rate and pressure of the compressed air were found to have insignificant influence on bulk properties of ALLP, such as geometric particle diameters and bulk tap density. However, increases in the inlet temperature increased bulk tap density and decreased aerosol performance ($P > 0.05$). Hence, process parameters were optimized and kept unaltered in subsequent experiments.

Poloxamer 188, L-leucine and AMK/TB were dissolved in distilled water. HSPC was added into the solution and was heated to 65-70°C to dissolve it. Coumarin (as a fluorescent marker) at 0.1% w/w on dry basis of ALLP was dissolved in methanol and the solution was transferred to aqueous dispersion at room temperature. The aqueous dispersion was diluted to distilled water to obtain 1.0%w/w of solid content and the resultant dispersion was either spray/freeze dried. For spray drying a laboratory spray-dryer (LSD-48, JISL, Mumbai, India) was used. Solutions were pumped into the drying chamber at a rate of 2 ml/min and pneumatically atomized through a 0.7 mm nozzle using aspiration at 100 % and compressed air at 1.5 kg/cm^2. The inlet temperature was set at 125 ± 5°C with outlet temperature of 65 to 70°C. The yield varied between 30 to 60 %. Freeze drying was carried out in a laboratory freeze dryer (DW1 0-60E; Heto Drywinner, Birkerod, Denmark) for 30 hrs after pre-freezing the samples at -180°C by use of liquid nitrogen. The porous cake thus formed was sized successively through #120 and #240 sieves (ASTM) and rotated in a planetary ball mill (200 r.p.m) without balls for 10 min for further deaggregation of the particles.

Each batch of ALLP was prepared three times and was evaluated for particle size, polydispersity, tap density and moisture content. The composition of ALLP and mean of three values of each parameter along with standard deviation are recorded in Table 4.1 and 4.2.

Table 4.1 Composition, Particle size, Span, Tap density, Theoretical mass median aerodynamic diameter, Residual moisture content and Equivalent moisture content of Tobramycin sulfate ALLP (Mean ± s.d., n=3).

Dry powders	*TB (%)*	*HSPC (%)*	*L-leucine (%)*	*Poloxamer188 (%)*	*VMD (µm)*	*Span*	*Tap density g/cm³*	*MMADt (µm)*	*RMC (%)*	*EMC* (%)*
A_1	30	52	15	3	7.624 ± 0.23	1.324 ± 0.09	0.039 ±0.021	1.506 ± 0.09	3.764 ± 0.31	1.365 ±0.125
A_2	40	42	15	3	11.022 ±0.115	1.627 ±0.003	0.046 ±0.066	2.364 ± 0.122	4.52 ± 0.90	0.916 ± 0.09
A_3	50	32	15	3	8.124 ±0.308	0.9 ±0.003	0.047 ±0.115	1.761 ± 0.206	4.113 ± 0.22	1.58 ±0.114
A_4	60	22	15	3	9.772 ±0.211	1.226 ±0.024	0.074 ±0.211	2.658 ± 0.062	5.012 ±0.554	1.87 ±0.652
B_1	30	52	15	3	14.490 ±0.352	2.745 ±0.006	0.049 ±0.044	3.207 ± 0.084	4.854 ±0.352	1.064 ±0.214
B_2	40	42	15	3	17.608 ±0.119	4.032 ±0.084	0.052 ±0.212	4.015 ± 0.124	5.055 ±0.731	1.679 ±0.346
B_3	50	32	15	3	20.01 ±0.308	3.114 ±0.031	0.054 ±0.102	4.650 ± 0.079	5.44 ±0.552	0.98 ±0.623
B_4	60	22	15	3	19.22 ±0.552	2.673 ± 0.11	0.06 ± 0.43	4.708 ± 0.313	5.776 ±0.365	1.06 ±0.087

A_1- A_4 & B_1- B_4 represents spray dried (SD) and freeze dried (FD) ALLP respectively.

* EMC was determined after vacuum drying for 72 hrs.

Table 4.2 **Composition, Particle size, Span, Tap density, Theoretical mass median aerodynamic diameter, Residual moisture content and Equivalent moisture content of Amikacin sulfate ALLP (Mean ± s.d., n=3).**

Dry powders	*AMK (%)*	*HSPC (%)*	*L-leucine (%)*	*Poloxa-mer188 (%)*	*VMD (μm)*	*Span*	*Tap density g/cm³*	*MMADt (μm)*	*RMC (%)*	*EMC* (%)*
A_1	30	52	15	3	8.044 ±0.439	1.728 ±0.159	0.047 ±0.003	1.757 ± 0.160	4.193 ±0.277	1.446 ±0.304
A_2	40	42	15	3	10.430 ±0.125	1.786 ±0.006	0.045 ±0.006	2.216 ± 0.122	4.40 ±0.655	1.916 ±0.146
A_3	50	32	15	3	7.956 ±0.348	1.677 ±0.003	0.047 ±0.005	1.728 ± 0.100	3.746 ±0.240	1.46 ±0.438
A_4	60	22	15	3	10.882 ±0.286	1.738 ±0.017	0.081 ±0.003	3.095 ± 0.034	4.883 ±0.356	2.013 ±0.070
B_1	30	52	15	3	16.490 ±0.683	3.853 ±0.143	0.050 ±0.002	3.701 ± 0.239	5.683 ±0.856	1.283 ±0.513
B_2	40	42	15	3	19.904 ±0.121	3.385 ±0.039	0.055 ±0.004	4.679 ± 0.197	6.02 ± .324	2.24 ±0.337
B_3	50	32	15	3	17.491 ±0.598	2.040 ±0.021	0.052 ±0.005	3.993 ± 0.059	5.36 ±0.353	1.69 ±0.251
B_4	60	22	15	3	17.531 ±1.019	2.497 ±0.124	0.077 ±0.003	4.872 ± 0.233	6.386 ±0.705	1.386 ±0.083

A_1- A_4 & B_1- B_4 represents SD and FD ALLP respectively.
* EMC was determined after vacuum drying for 72 hrs.

4.4 OPTIMIZATION OF FORMULATION COMPONENTS

Quantitative aspects of the effects and relationships among various formulation components of high therapeutics payload ALLP produced by spray drying technique are investigated using response surface methodology.

A 3-factor, 5-level central composite design was used for the optimization procedure. This design is suitable for exploring quadratic response surfaces and constructing second-order polynomial models. The complete design consisted of 16 experimental points that included eight vertex points, six axial points and two replications at the centre point. The non-linear quadratic model generated by the design is as follow:

$$Y= \beta_0+ \beta_1X_1+ \beta_2X_2+ \beta_3X_3+ \beta_{12} X_1X_2+ \beta_{13}X_1X_3+ \beta_{23}X_2X_3+ \beta_{11}X_1^{\,2}+ \beta_{22}X_2^{\,2}+ \beta_{33}X_3^{\,2}$$

------ Equation (4.1)

Where, Y is the measured response (dependant variable) associated with each factor-level combination; expressed in terms of fine particle fraction (FPF), β_0 is an intercept, β_1, β_2, β_3, β_{12}, β_{13}, β_{23}, β_{11}, β_{22} and β_{33} are the regression coefficients. X_1, X_2 and X_3 are the (independent factors studied) percent weight by weight of L-leucine, TB/AMK and poloxamer-188 respectively. The independent factors and the dependent variable used in the design are listed in Table 1. The JMP (Version 5.1, SAS Institute Inc, Cary, NC, USA) program was used for design of experiment and analysis of this second-order model. Sigma plot 8.0 was used for drawing of three dimensional response surface and contour plots.

Table 4.3 Variables in Central Composite Design

X_i	Independent variables (%w/w)	Coded values					Response (Y)
		-2	-1	0	1	2	
X_1	L-Leucine	0	5	10	15	20	Fine Particle Fraction (FPF)
X_2	TB/AMK	20	30	40	50	60	
X_3	Poloxamer 188	1	3	5	7	9	

Table 4.4 Matrix of central composite design of Tobramycin sulfate and response of each experimental run

Exp. No.	RSM pattern	Factors			Actual response (Y,FPF)	Predicted response (Y_P)
		X_1	X_2	X_3		
1	00a	0	0	-2	44.50	48.03
2	-++	-1	1	1	43.18	42.58
3	000	0	0	0	55.03	56.20
4	00A	0	0	2	52.06	51.42
5	0a0	0	-2	0	53.58	54.62
6	+--	1	-1	-1	60.80	58.49
7	0A0	0	2	0	40.56	42.41
8	000	0	0	0	54.48	56.20
9	+-+	1	-1	1	62.47	60.66
10	+++	1	1	1	56.05	55.42
11	A00	2	0	0	61.78	64.84
12	-+-	-1	1	-1	42.47	41.37
13	a00	-2	0	0	42.01	41.85
14	++-	1	1	-1	60.51	56.21
15	--+	-1	-1	1	51.13	52.52
16	---	-1	-1	-1	50.62	48.34

A, a – Higher and lower axial values respectively.

Table 4.5 Matrix of central composite design of Amikacin sulfate and response of each experimental run

Exp. No.	RSM pattern	Factors			Actual response (Y,FPF)	Predicted response (Y_P)
		X_1	X_2	X_3		
1	00a	0	0	-2	45.23	45.44
2	-++	-1	1	1	39.56	42.62
3	000	0	0	0	54.08	53.46
4	00A	0	0	2	54.16	53.50
5	0a0	0	-2	0	49.54	49.44
6	+--	1	-1	-1	59.71	57.10
7	0A0	0	2	0	41.35	40.99
8	000	0	0	0	53.3	53.46
9	+-+	1	-1	1	61.26	61.35
10	+++	1	1	1	56.06	54.01
11	A00	2	0	0	66.24	68.85
12	-+-	-1	1	-1	38.47	38.83
13	a00	-2	0	0	43.37	40.30
14	++-	1	1	-1	59.03	58.82
15	--+	-1	-1	1	52.13	52.79
16	---	-1	-1	-1	37.44	39.94

A, a – Higher and lower axial values respectively.

4.5 CHARACTERIZATION OF AERODYNAMICALLY LIGHT AND LARGE PARTICLES

4.5.1 Determination of Particle Size and Polydispersity

The particle size was determined by laser diffractometry (Malvern MasterSizer 2000 series, Malvern Instruments, Worcestershire, UK) using the Hydro 2000SM sampling unit. The apparatus consisted of a He-Ne laser (5 mw) and a sample holding cell of 50 ml capacity. Each sample in sufficient quantity was dispersed in isopropyl alcohol so as to achieve obscuration range between 10-20%. Samples were kept under stirring using a blade stirrer at 1000 rpm to keep particles in suspended form and the measurements were recorded for VMD, which is related to the mass median diameter by the density of the particles

(assuming a size independent density for the particles). The polydispersibility of powder was defined from span (Chew et al, 2002).

$$\text{Span} = \frac{[D(v, 90) - D(v, 10)]}{[D(v, 50)]} \quad \text{---------- Equation (4.2)}$$

Where D (v, 90), D (v, 10) and D (v, 50) are equivalent volume diameters at 90, 10 and 50% cumulative volume, respectively.

4.5.2 Determination of Tap Density

The powder density (ρ) was evaluated by tap density measurements. Assuming a perfect packing, the tap density of monodisperse spheres is approximately a 21% underestimate of the particle density due to the void spaces between particles. In case of polydisperse particles, the void spaces are reduced but this is probably counterbalanced by incomplete packing (Vanbever et al, 1999 and Bosquillon et al, 2004). The theoretical mass median aerodynamic diameter (MMADt) of individual particles was calculated based on the following definition:

$$MMADt = \sqrt{(\rho/\rho_1)} * d \quad \text{---------- Equation (4.3)}$$

Where $\rho_1 = 1$ g/ cm^3.

ρ = tapped density

d= geometric particle size

The tapped densities (ρ) were measured in a 10-ml glass measuring cylinder filled with fixed volume of powder. The tapped density was determined after 500 taps from a constant height.

4.5.3 Determination of Moisture Content

The weight loss on heating was analyzed by halogen moisture analyzer (HR 73 moisture analyzer, Mettler Toledo, Illinois, USA)). 0.5 g of the sample was placed on the pan and dried to constant weight at 50°C. The weight loss on heating was expressed as a percentage of the initial weight.

4.5.4 Determination of Crystallinity

The thermal properties were analyzed using differential scanning calorimetry (DSC) (DSC60, Shimadzu, Shimadzu Corporation, Japan) with TA- 60 WS work station. Thermograms were analyzed using shimadzu TA-60 software. An empty aluminum pan was used as the reference for all measurements. A sample (2-4 mg) of powder was placed in hermetically sealed aluminum pan and scanned at a rate of 10°C/min from 25°C to 300°C .The onset and peak temperatures and enthalpy of transition (ΔH) were determined for each peak.

4.5.5 Characterization of Morphological Features

The morphology was examined by scanning electron microscopy (SEM) (JSM-5610LV, JEOL, Japan). Samples were attached to sample stubs using double sided tape, and then viewed using an accelerating voltage of 15 kilovolt at the magnification of 250X to 5000X. Particle traits and surface topography were assessed using image analysis software (Image Proplus 5.0, Media Cybernetics, USA). Image analysis of the SEM pictures was conducted on a fixed area selected on the particle flat base in order to avoid tilting angle shadow effect. The traits such as roundness and elongation ratio were calculated as described below

Roundness: Reports the roundness of each object, as determined by the following formula: $(perimeter^2) / (4 * \Pi * area)$.

Elongation ratio: Reports the ratio between the Feret max (reports the longest caliper length) to the Feret min (reports the average caliper length) and were calculated from 16 caliper measurements at 6°C intervals around the particle. These two measurements were not necessarily at right angles to each other.

Three dimensional surface plots, which describe the surface topography of particles, were drawn by scanning on the selected area of the image, an up and down, line showing the variability of gray level as a function of the position. Ten surface plots were drawn on each image and topographical features *viz.* fractal dimension, heterogeneity, and clumpiness; the descriptors of the texture of the surface were calculated and are defined as follows

Fractal dimension: Calculated as 1 minus the slope of the regression line obtained when plotting the log of the perimeter (using a particular stride) against the log of the stride length, as calculated with multiple starting points in the outline for the strides.

Heterogeneity: Reports the fraction of pixels that vary more than 10% from the average intensity of the object.

Clumpiness: Derived from heterogeneity measurement; the fractions of heterogeneous pixels remaining in an object after an erosion process reflecting the object texture.

4.5.6 Drug Assay

4.5.6.1 Estimation of Tobramycin sulfate

TB content in formulations was estimated by dissolving equivalent quantity of powder containing 55 mg of TB in methanol; drug was extracted into the aqueous media by addition of equal volume of distilled water into it and incubated in water bath at 65°C for 30 minutes. The resultant system was centrifuged at 10,000 rpm for 10 minutes (Sigma

Laboratory centrifuge, 3K 30, Osterode, GmBH), supernatant was separated and volume was made up with distilled water. The drug content was determined by using an HPLC system with UV detection as previously described (United States Pharmacopoeia, 2004). The HPLC system was composed of a pump (P-680, Dionex), a simple 20-µl loop injector (Reodyne 7125) and a UV spectrophotometric detector (UVD 170U, Dionex). The separation was carried out on a Thermohypersil-ODS (4.6 by 25 cm [inside diameter]; particle size, 10 µm; Thermo Electron Corporation, Bellefonate, PA, USA). The mobile phase was tris(hydroxymethyl)aminomethane(0.25%w/v aqueous solution)-1N sulfuric acid- acetonitrile (40:1:59[vol/vol/vol]), and the flow rate was 1.2 ml/min. The column effluent was monitored at 365 nm and at 0.005 absorbance units full-scale. Chromatography was performed at room temperature. The procedure for the determination of TB concentrations was based on derivatization of the TB with 2, 4-Dinitrofluorobenzene. The data was analyzed by Chromleon 6.5 software.

4.5.6.2 Estimation of Amikacin sulfate

AMK content in spray dried (SD) and freeze dried (FD) formulations was estimated by dissolving equivalent quantity of powder containing 50 mg of AMK in methanol; drug was extracted into the aqueous media by addition of equal volume of distilled water into it and incubated in water bath at 65°C for 30 minutes. The resultant system was centrifuged at 10,000 rpm for 10 minutes (Sigma Laboratory centrifuge, 3K 30, Osterode, GmBH), supernatant was separated and volume was made up with distilled water. The drug content was determined by using an HPLC system with UV detection as previously described (British Pharmacopoeia, 2004). The HPLC system was composed of a pump (P-680, Dionex), a simple 20-µl loop injector (Reodyne 7125) and a UV spectrophotometric detector (UVD 170U, Dionex). The separation was carried out on a Thermohypersil-ODS (4.6 by 25 cm [inside diameter]; particle size, 10 µm; Thermo Electron Corporation, Bellefonate, PA, USA). The mobile phase was methanol -potassium phosphate buffer (70:30[vol/vol] pH 6.5), and the flow rate was 1.0 ml/min. The column effluent was monitored at 340 nm and at 0.005 absorbance units full-scale. Chromatography was performed at room temperature. The procedure for the determination of AMK concentrations was based on derivatization of the AMK with 2, 4, 6-trinitrobenzene sulphonic acid. The data was analyzed by Chromleon 6.5 software.

4.5.7 Characterization of Aerosol Performance

The *in- vitro* aerosol dispersion was determined using an eight stage, nonviable Andersen cascade impactor with a preseparator (Graseby-Andersen, Atlanta, GA, USA) operating at

an airflow of 28.3, L/min for 10 s. The cutt-off aerodynamic diameters of stages 0 to 7 were 9, 5.8, 4.7, 3.3, 2.1, 1.1, 0.7, and 0.4. The impaction plates were pre-coated with a 2% w/v of hydroxypropylmethylcellulose (4000 cps) gel in water to prevent particle bounce and re-entrainment. A size '2'hard gelatin capsule (Universal capsules, Mumbai, India) was filled with 20 mg of powder and aerosolized using Rotahaler (Cipla limited, Mumbai, India). Ten capsules were shot for each impaction with each capsule had air drawn through it for 10 secs. The powder deposited in induction port, preseparator, individual impaction plates, and powder remaining in capsule and inhaler device was recovered by immersing each part in methanol. Fluorescence of each solution due to coumarin was determined using a Shimadzu spectroflourometer RF 540 (Shimadzu corporation, Japan) at $\lambda_{excitation}$= 458 nm and $\lambda_{emission}$= 545 nm. Each measurement was repeated thrice.

Emitted dose (ED), fine particle fraction (FPF), experimental mass median aerodynamic diameter ($MMAD_e$) and geometric standard deviation (GSD) of ALLP was calculated according to USP 27 NF 22. FPF was calculated from ratio of the total mass of powder (R) having particle size below 5 μm to the total mass (ΣA) of powder delivered from the mouthpiece of the inhaler into the apparatus i.e

$$FPF = R/\Sigma A \text{ ---------- Equation (4.4)}$$

The cumulative mass of powder less than the stated size of each stage of the Andersen impactor was calculated and plotted on a log probability scale, as percent of total mass recovered in the impactor against the effective cut-off diameter. The $MMAD_e$ of the particles is defined from this graph as the particle size at which the line crosses the 50% mark and the GSD was calculated as below

$$GSD = \sqrt{\frac{Size\ X}{Size\ Y}} \text{ --------- Equation (4.5)}$$

Where size *X* is the particle size for which the line crosses the 84.13% mark and size *Y* the 15.87% mark.

Capsule and device retention is defined as the mass fraction of the powder remaining in the capsules and the device. Impaction loss is defined as the mass fraction of the powder collected at the induction port, preseparator and up to stage 2 of the cascade impactor. FPF, retention, and impaction loss were all referenced against the recovery (i.e., total dose=emitted dose + device and capsule retention) and were expressed as the means of triplicate runs (n = 3). Data were subjected to analysis of variance (ANOVA) and Student's *t* test (Microsoft Excel version 2003) with probability values of less than 0.05 considered as statistically significant.

4.6 RESULTS AND DISCUSSION

4.6.1 Preparation and Characterization of Spray and Freeze Dried Aerodynamically Light and Large Particles

ALLP of TB and AMK was prepared by varying proportions of HSPC and drug. Spray and freeze drying parameters were previously optimized and the same operational parameters were used to prepare ALLP. Each batch of ALLP was prepared three times and was evaluated for particle size, polydispersity, tap density and moisture content. The composition of ALLP and mean of three values of each parameter along with standard deviation are recorded in Table 4.1 and 4.2. Marginal differences were observed in traits such as tap density and moisture content of ALLP containing 30-50%w/w of drug. Further increase in drug proportion resulted increase in density of ALLP. Both the spray and freeze drying techniques were found to be reproducible with high therapeutic payload ALLP. Significant difference in particle size (VMD) and polydispersity observed between SD and FD ALLP. The 'span' measures the width of the particle size distribution (polydispersity) and small span value indicated narrow particle size distribution (Chew et al, 2002). Precise control of spray drying process may be the reason of smaller span value for SD-ALLP and uniform particle size, shape, morphology, and density (Hickey et al, 1996). On contrary, freeze drying followed by conventional particle size reduction may have contributed to large span value to FD-ALLP as shown in Figure 4.1 and 4.2.

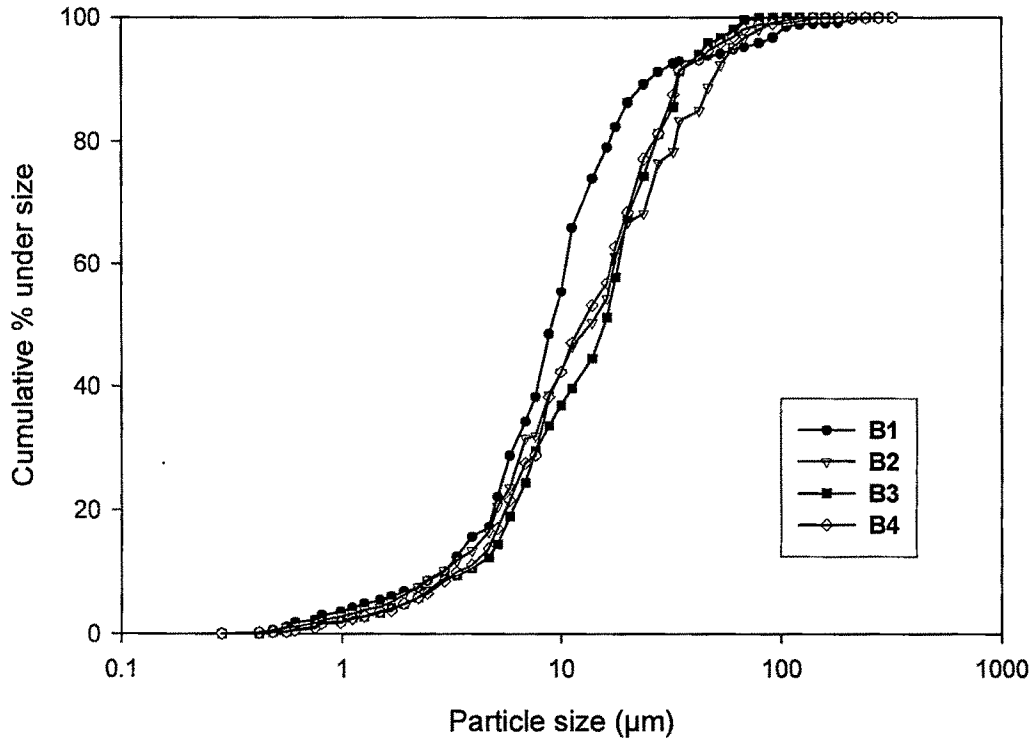

(A)

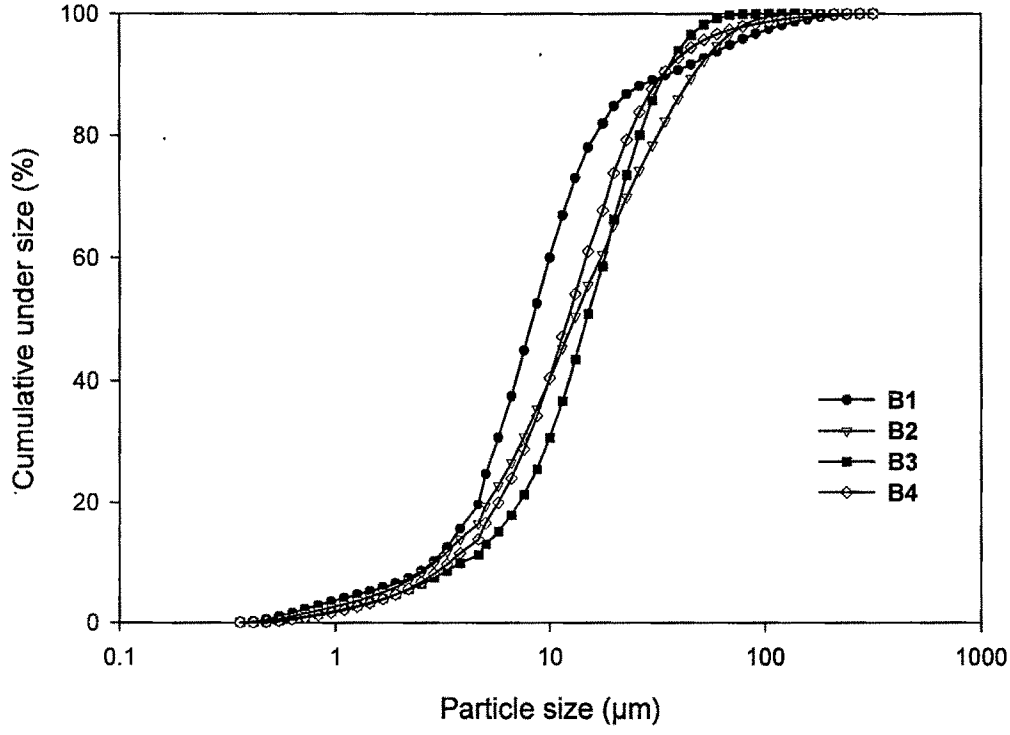

(B)

Figure 4.1 Particle size distribution of freeze dried TB (A) and AMK (B) ALLP determined by laser diffraction.

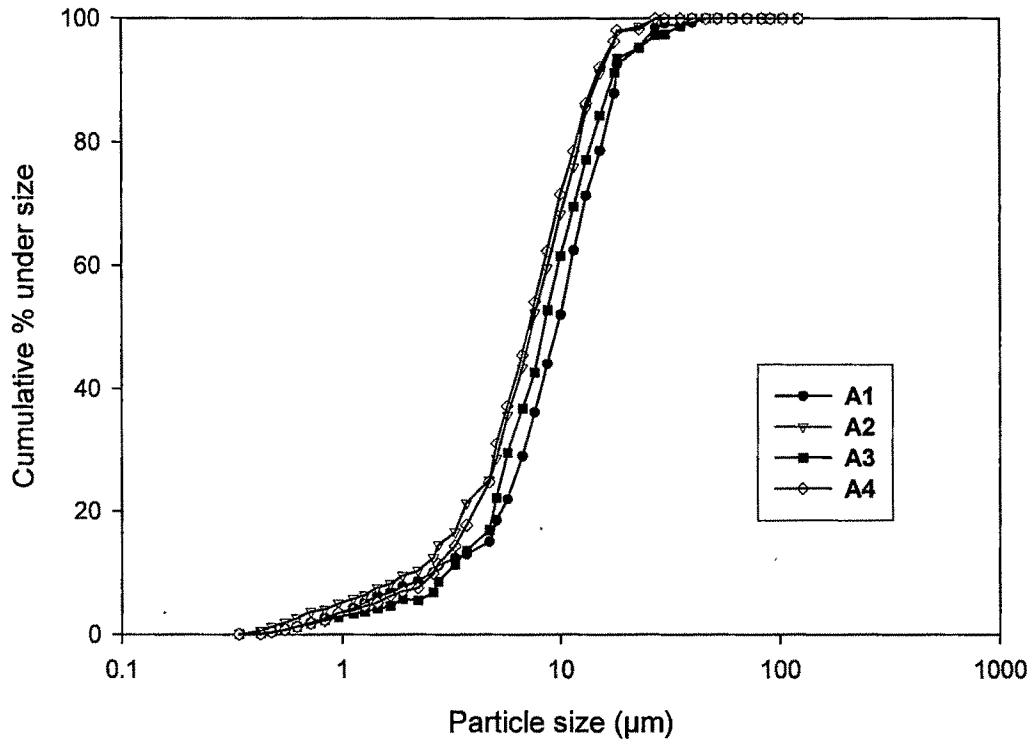

(A)

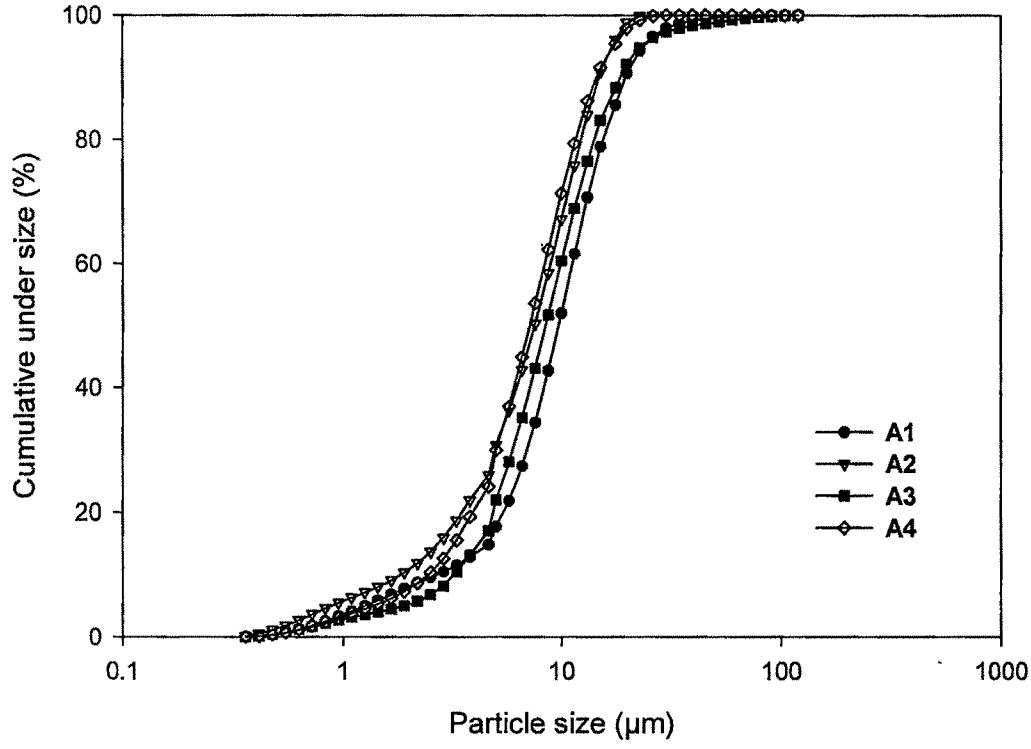

(B)

Figure 4.2 Particle size distribution of Spray dried TB (A) and AMK (B) ALLP determined by laser diffraction.

SD-ALLP of both TB and AMK were consistently drier then FD-ALLP. However, on subsequent vacuum drying, both ALLP reached same level of moisture content. Negligible weight loss on heating was observed for both vacuum dried ALLP (Table 4.1 and 4.2).

DSC thermograms for FD and SD-ALLP containing TB revealed an endothermic peak between 274°C to 278°C, corresponding to the melting endotherm of pure TB at 272.17°C (Figure 4.3 A). The molar heat of fusion value for SD-ALLP (ΔH 199.49mJ) is higher then pure TB (ΔH 8.87 mJ), this could be due to crystallization of TB during the DSC run in molten formulation excipients (HSPC/poloxamer 188/L-leucine).

A single endothermic peak was observed around 264 to 269°C in both FD and SD AMK – ALL samples (Figure 4.3 B), which corresponded with the melting endotherm of AMK (268.86°C). The onset and peak temperatures and enthalpy of fusion (ΔH) were similar for each sample. The SD and FD samples showed negligible differences in molar heat of fusion and peak temperature. The thermograms suggest that manufacturing process do not result into any interaction between components of ALLP and do not modify crystallinity of the drug.

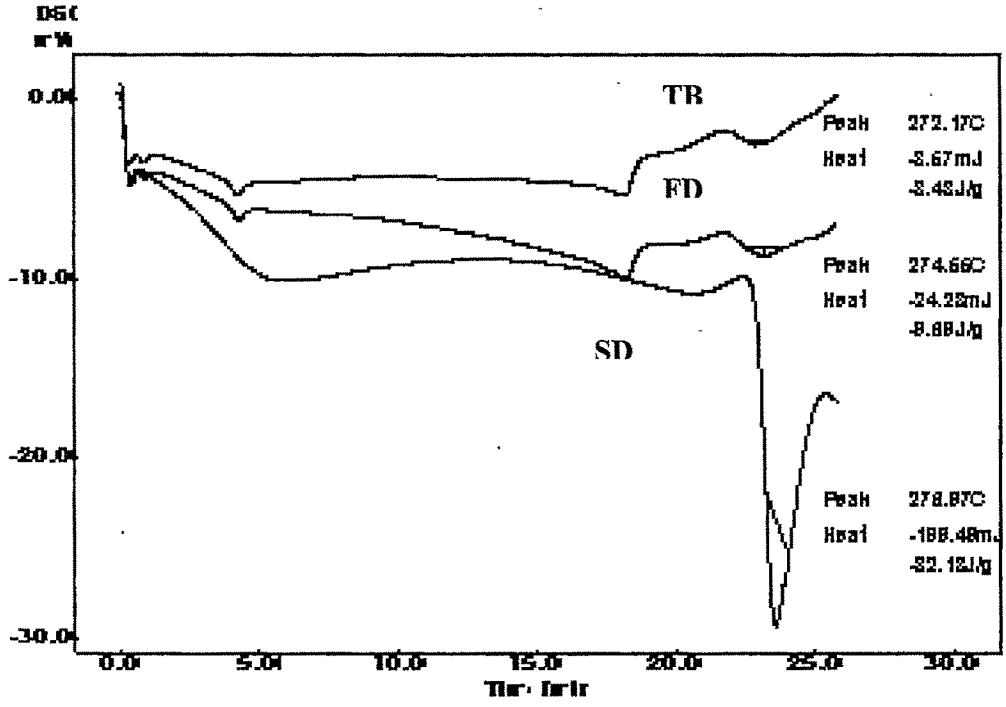

(A)

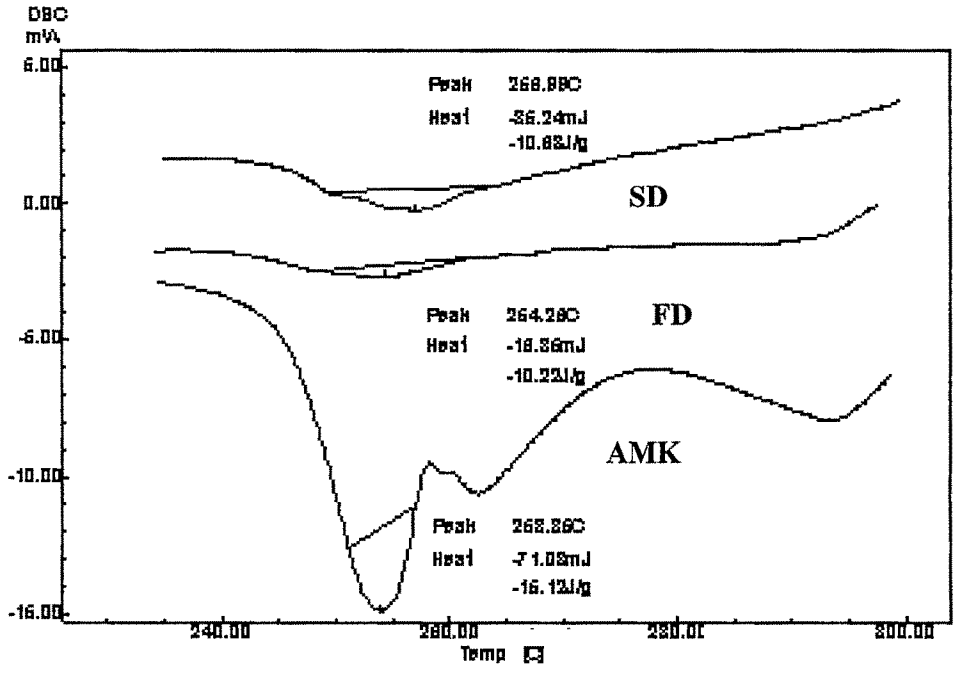

(B)

Figure 4.3 DSC thermograms of freeze dried (FD) and spray dried (SD) ALLP of TB (A) and AMK (B)

SEM photographs of SD and FD ALLP of TB and AMK are shown in Figure 4.4 & 4.5 respectively and image analysis data are recorded in Table 4.6. SD-ALLP were dimpled spherical shape with roundness value of 1.048± 0.032, 1.066 ± 0.028 and elongation ratio of 1.206 ± 0.164, 1.263 ± 0.178 for TB and AMK respectively. However, FD- ALLP were irregular morphologies with large roundness value of 1.812± 0.338, 1.707 ± 0.454 and elongation ratio of 2.422± 0.984, 2.633 ± 1.084 for TB and AMK respectively. Increased elongation ratio of FD -ALLP may be due to the growth of the longest axis of the crystals accelerated by process of sublimation of ice crystals from the frozen sample lattice (Larhrib et al, 2003).

Topographical features of ALLP were derived from image analysis of SEM photographs by Image Proplus 5.0 and are shown in Figure 4.6A & 4.6B. Figures suggest varying degrees of surface roughness at different locations on surface of SD and FD ALLP. The surface fractal dimension, which represents degree of particle surface corrugation (Chew et al, 2005) was determined from the texture of the images of SD and FD ALLP surfaces and is recorded in Table 4.6. The results indicate that a significant ($p < 0.05$) reduction of roughness with SD-ALLP when compared to FD-ALLP. Higher value of heterogeneity and clumpiness for FD-ALLP further suggests high degree of roughness in contrast to SD-

ALLP. These variations were probably related to differing in the processes and kinetics of particle formation. Controlled spray-drying process parameters, such as drying temperature, feed rate, aspiration volume etc., may have contributed to the formation of spherical and smooth particles (Hickey et al, 1996).

The actual TB and AMK content of the ALLP analyzed by HPLC was between 96.0 and 102.0% relative to the theoretical titer of 100% and was taken into account for calculation purposes.

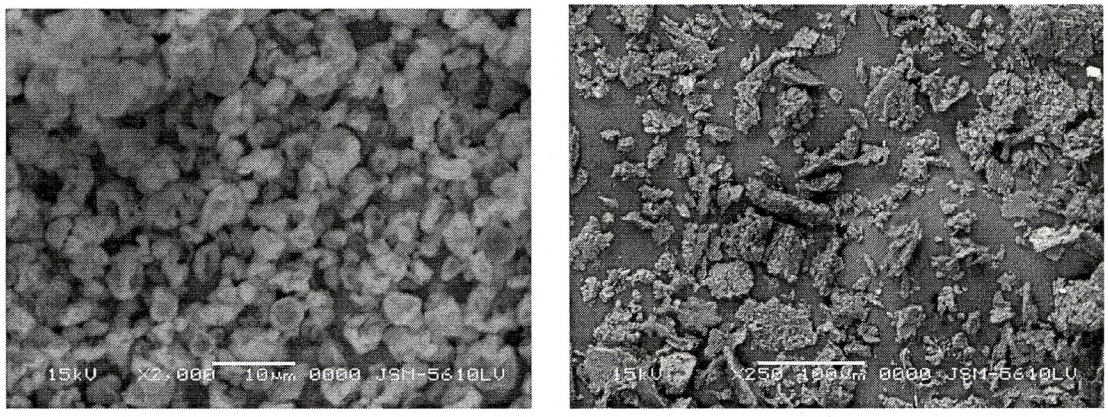

(A) (B)

Figure 4.4 Scanning electron micrographs of SD (A) and FD (B) TB-ALLP.

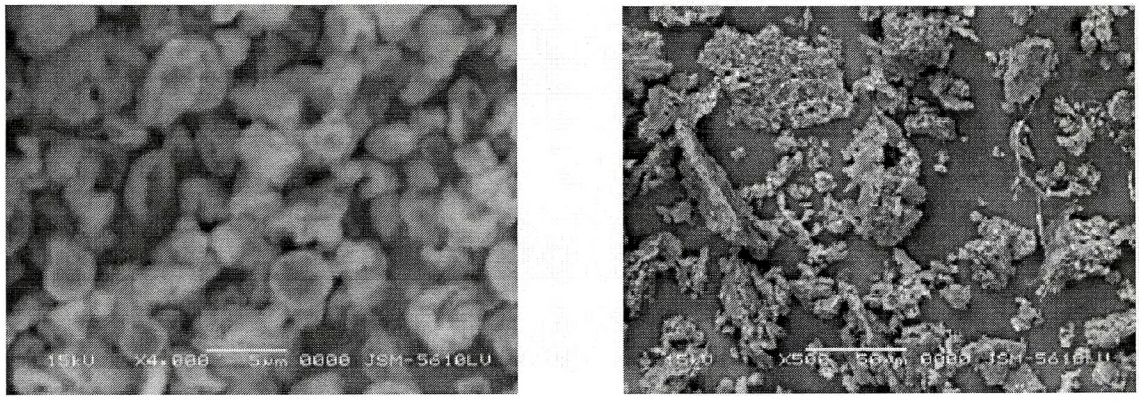

(A) (B)

Figure 4.5 Scanning electron micrographs of SD (A) and FD (B) AMK-ALLP.

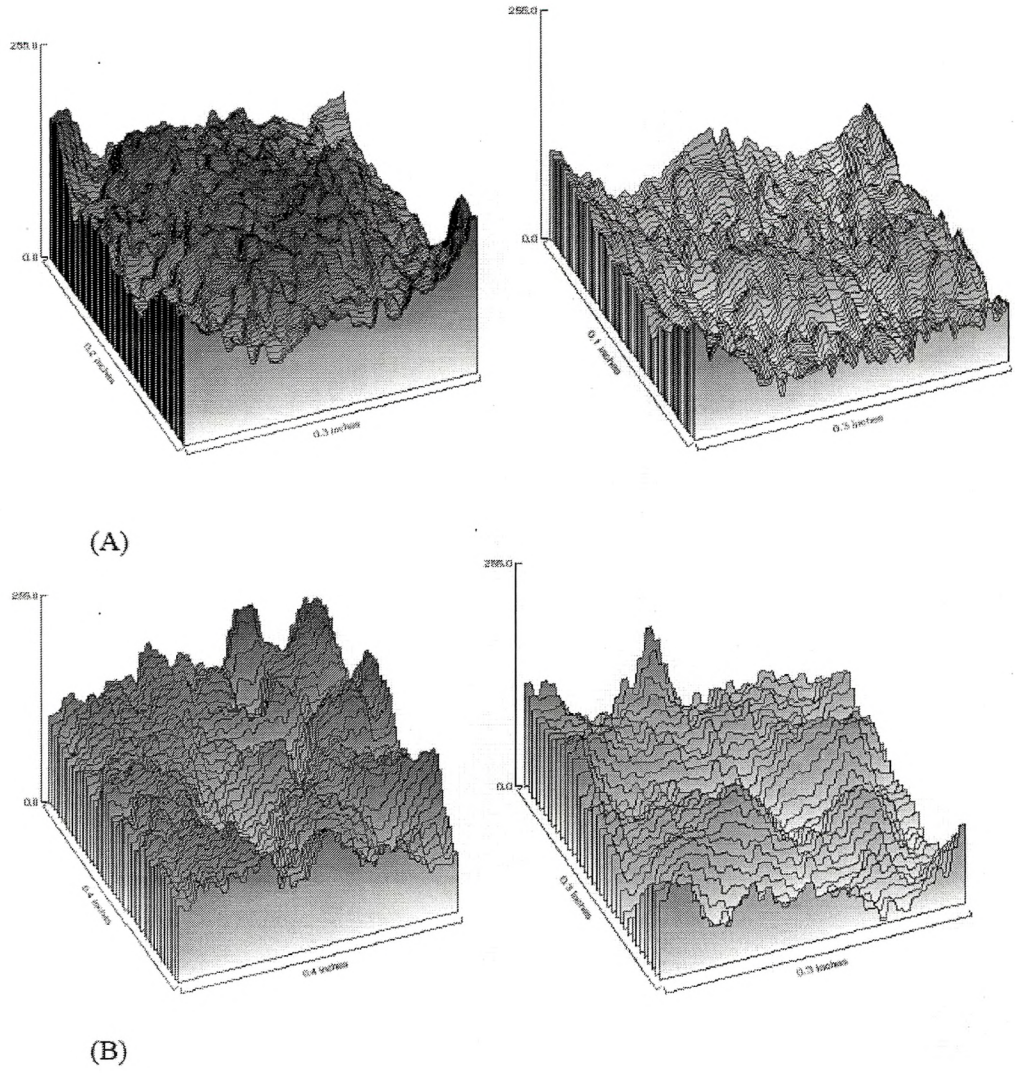

Figure 4.6 3-D surface plots of SD (A) and FD (B) ALLP.

Table 4.6 Topographical features of SD and FD particles measured by SEM image analysis (Mean ± s.d., n=10)

ALLP		Roundness	Elongation ratio	Fractal dimension	Heterogeneity	Clumpiness
SD-ALLP	TB	1.048 ± 0.032	1.206 ± 0.164	1.036 ± 0.007	0.289 ± 0.067	0.045 ± 0.026
	AMK	1.066 ± 0.028	1.263 ± 0.178	1.058 ± 0.006	0.312 ± 0.092	0.041 ± 0.033
FD-ALLP	TB	1.812± 0.338	2.422 ± 0.984	1.582 ± 0.22	0.513 ± 0.094	0.192 ± 0.106
	AMK	1.707 ± 0.454	2.633 ± 1.084	1.766 ± 0.214	0.404 ± 0.112	0.179 ± 0.125

Table 4.7 Summary of In-vitro aerosol deposition data of ALLP produced by spray and freez drying (Mean ± s.d., n=3).

ALLP		**RD (mg)**	**ED (%)**	**FPF (%)**	**Impaction loss (%)**	**MMADe (µm)**	**GSD**
SD-ALLP	TB	193.212 ± 1.684	88.022 ± 1.033	59.687 ± 2.122	24.938 ± 1.067	2.24 ± 0.142	1.642 ± 0.111
	AMK	191.717 ± 2.173	86.759 ± 0.438	56.958 ± 1.125	26.607 ± 0.988	2.133 ± 0.115	1.524 ± 0.201
FD -ALLP	TB	195.02 ± 2.061	69.970 ± 1.542	35.287 ± 2.662	35.921 ± 2.024	2.652 ± 0.124	2.77 ±0.092
	AMK	190.226 ± 1.313	73.940 ± 1.231	31.266 ± 1.435	38.492 ± 1.097	2.754 ± 0.117	2.883 ±0.105

4.6.2 Aerosolization properties of SD and FD ALLP

The *in- vitro* aerosol deposition data are recorded in Table 4.7. It was observed that the recoverable powder mass for all formulations were with in the range of 95.0 ± 1% of mass of powder filled into capsules, suggesting the method of washing and analyzing was accurate and reproducible.

Capsule and Device Retention

The percent mass distribution of SD and FD ALLP on cascade impactor is shown in Figure 4.7A and 4.7B for TB and AMK ALLP respectively. The capsule and device retention of the FD-ALLP was significantly higher ($p < 0.05$) than those of SD-ALLP. The mass of powder delivered from the mouthpiece of the Rotahaler (ED) varied from 86-88% with SD-ALLP to 69-74% for FD-ALLP. The results indicate that 14-17% of recoverable dose of FD-ALLP was retained in the capsules and/or in the inhaler device. The reason for lower emission may be poor flow properties of FD-ALLP contributed by traits such as large elongation ratio and irregular morphologies of FD-ALLP.

Impaction Loss

The mass distribution data shown in Figure 4.7A & 4.7B suggest 10-12 % higher impaction loss for FD-ALLP than SD-ALLP. The lower impaction loss for the SD-ALLP when dispersed by the Rotahaler indicated that these particles were easier to disperse and the agglomerates formed during dispersion were much smaller than those of the FD-ALLP. It may be partly due to influence of traits such as large particle size, wide particle size distribution (high span value), and irregular morphologies with high values of aspect ratio and roundness. FD-ALLP are larger (as measured by MMADt) and possesses a larger span: this means that there larger particles compared to SD-ALLP. The large particles are deposited in the first stages of the cascade impactor. This may be reason for high impaction loss and deposition of powder in upper stages of cascade impactor of FD-ALLP.

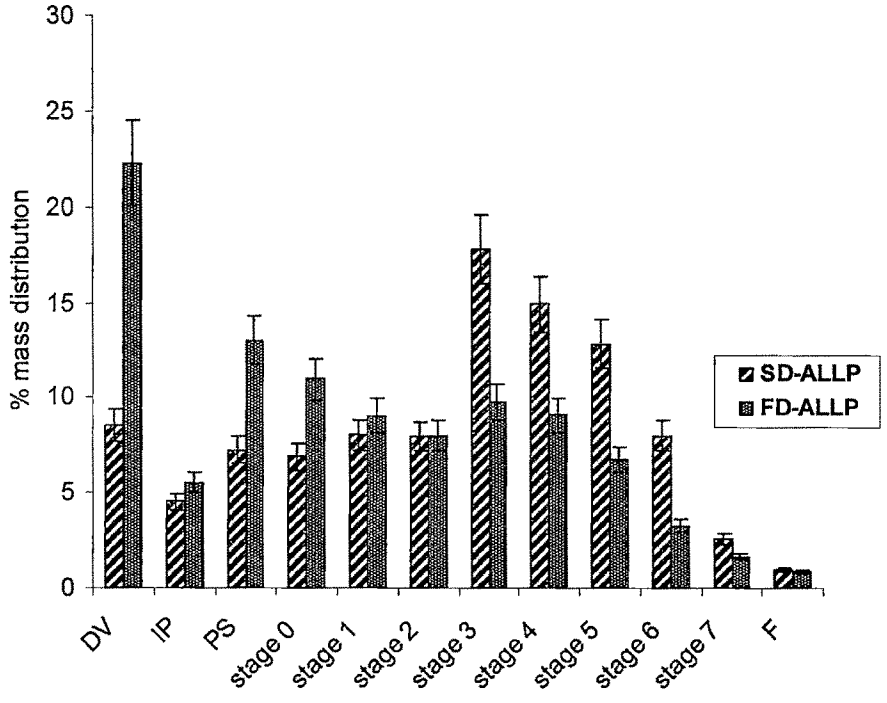

(A)

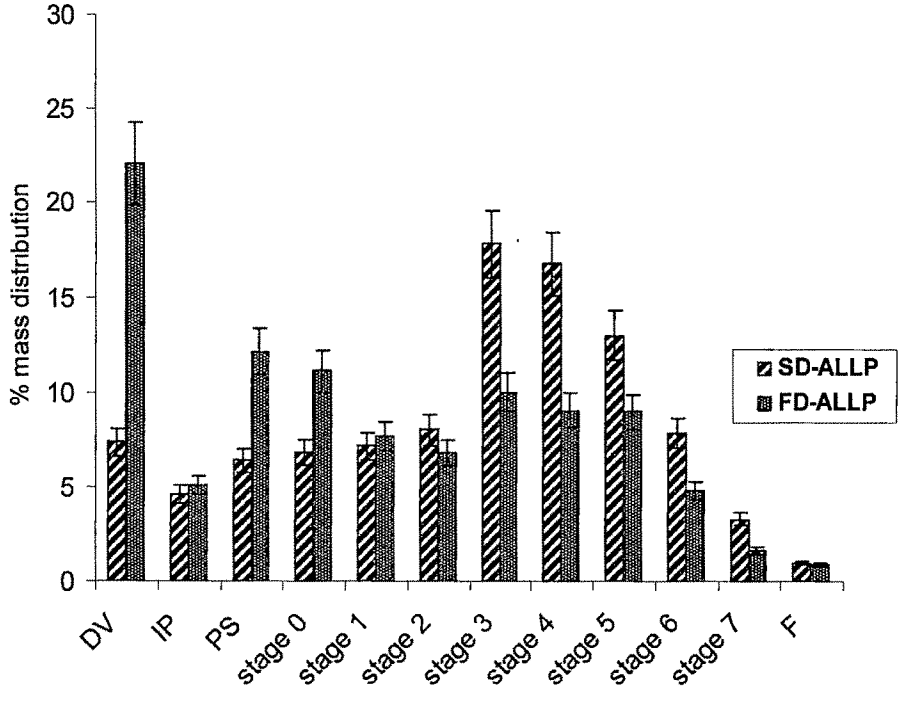

(B)

Figure 4.7 **Comparative percent mass distribution of SD and FD-ALLP of TB (A) and AMK (B) in cascade impactor (Mean ± s.d., n=3).**

Fine particle fraction

The fine particle fraction of SD-ALLP is significantly higher ($p< 0.05$) than FD-ALLP, a better dispersibility of particles of < 5μm (stage 2 and the filter) was observed for SD-ALLP, 56-60% vs. 31-35%. Once a powder is dispersed, the FPF is determined by the aerodynamic diameter of the particles in the aerosol. Despite having significant difference in geometric size, both SD and FD-ALLP displayed marginal difference in aerodynamic diameters. The smaller aerodynamic diameter of FD-ALLP is due to higher drag force on the rough surface (Chew et al, 2001). The improvement of FPF with SD-ALLP was due to i) reduction in the capsule and device retention of the SD-ALLP and/or ii) increase in the powder dispersibility, that is, the amount of fine particles in the aerosol cloud per emitted dose. High fine particle fraction of SD-ALLP may also have been contributed by the spherical shape of SD-ALLP and lesser degree of particle surface corrugation (Table 4.6; Figure 4.6A & 4.6B). A little surface corrugation is reported to cause considerable improvement in the aerosol performance of the powder (Chew et al, 2005). Surface corrugation is known to decrease particle-particle interactions in two ways; the first, the asperities prevent close contact between particles and effectively increase the inter-particle distance and the second, the asperities reduce the total area accessible for interaction. Another possible reason for improved aerosol performance may be lower electrostatic charges on ALLP produced by spray drying. The reason for higher electrostatic charges on FD- ALLP may be due to size reduction of lyophilized cake.

ALLP produced by spray-drying technique was found to have better aerosol performance than FD-ALLP. Traits and topographical features of ALLP, such as particle size, polydispersity, elongation ratio, roundness, shape, and degree of surface roughness (surface corrugation) are found to significantly influence by the technique of production. SD-ALLP were shown to possess higher FPF, lower impaction loss, and less capsule and device retention. Hence, the carefully selection and optimization of method of preparation will significantly improve the deposition of drug to the lower airways needed in CF and non-CF bronchiectasis diseases. ALLP produced be spray drying has been selected to further investigate the quantitative aspects of the effects and relationships among various formulation components of high therapeutics payload ALLP, which are profoundly influenced by several formulation components.

4.6.3 Optimization of Formulation Components of Aerodynamically Light and Large Particles Prepared By Spray Drying

ALLP were prepared by spray-drying technique using L-leucine/drug/poloxamer-188/HSPC. Process parameters, such as feed rate and pressure of the compressed air were found to have insignificant influence on bulk properties of ALLP, such as geometric particle diameters and bulk tap density. However, increases in the inlet temperature increased bulk tap density and decreased aerosol performance ($P > 0.05$). Hence, process parameters were optimized and kept unaltered in subsequent experiments. The effect of the proportion of formulation components on the aerosol performance of ALLP was investigated. ALLP with similar density, geometric size and MMADt were obtained with varying proportion of HSPC in the formulation. Sixteen batches of ALLP were prepared by spray drying process using a 3-factor, 5-level central composite design varying three independent variables (percent weight by weight of L-leucine (X_1), TB/AMK(X_2) and poloxamer-188 (X_3) of the formulation according to Table 4.3. The influence of these variables on observed response (Y, fine particle fraction) is recorded in Table 4.4 and 4.5 for TB and AMK respectively. Each batch of ALLP was prepared three times and was evaluated for particle size, polydispersity (span), tap density and moisture content. The composition of ALLP and mean of three values of each parameter along with standard deviation are recorded in Table 4.4 and 4.5. The maximum responses were 62.47% & 66.24% and minimum responses were 40.57% & 37.44% for TB and AMK ALLP respectively. The mathematical relationship for TB and AMK in terms of a polynomial equation relating the response Y and independent variables was: $Y= 56.2068 + 5.7481\ X_1 - 3.0531\ X_2 + 0.8468\ X_3 + 1.1737\ X_1 X_2 - 0.5012\ X_1 X_3 - 0.7412\ X_2 X_3 - 0.7149\ X_1^2 - 1.9212\ X_2^2 - 1.6187 X_3^2$ and $Y= 53.464 + 7.137\ X_1 - 2.112\ X_2 + 2.013\ X_3 + 0.707\ X_1 X_2 - 2.149\ X_1 X_3 - 2.265\ X_2 X_3 + 0.278\ X_1^2 - 2.061\ X_2^2 - 0.998 X_3^2$ respectively. Equations express the quantitative effect of the individual formulation components (X_1, X_2, and X_3) and combination thereof on the response (Y) in terms of interaction coefficients. The values of the coefficients X_1 to X_3 are related to the effect of these variables on the response (Y). Coefficients with more than one factor term and those with higher order terms represent interaction terms and quadratic relationships respectively. A positive and negative signs suggest a positive and negative effect on response respectively. The theoretical (predicted) values and the observed values were in reasonably good agreement as seen from Table 4.4 and 4.5. The significance of the ratio of mean square variation due

to regression and residual error was tested using analysis of variance (ANOVA). The ANOVA indicated a significant ($P < 0.05$) effect of factors on response. Lack of fit was not significant ($p = 0.08$, $p = 0.13$) and regression was strongly significant ($p = 0.01$, $R^2 = 0.92$; $p = 0.001$, $R^2 = 0.96$), so it was concluded that the second-order model adequately approximated the true surface. The estimated second-order RSM indicated that TB/AMK proportion affected negatively, while the L-leucine and poloxamer -188 proportion was affected positively. One can also see that X_1 was the most significant factor.

The relationship between the dependent and independent variables was further elucidated using contour and response surface plots. The effect of X_1 and X_2 and their interaction on Y at a fixed level of X_3 (5% w/w) are given in Figure 4.8A & 4.8B. As shown in Figure 4.8A, at lower levels of X_1 (amount of L-leucine added below 10%w/w), Y increases from 23.36% to 54.62% when the amount of TB (X_2) decreases from 60 to 20 %w/w. Similarly, at higher levels of X_1(on and above 15% w/w), Y decreases from 58.57% to 49.79% when X_2 increases from 20 to 60% w/w. Figure 4.9A & 4.9B, shows that at lower levels of X_1, Y increases from 25.0% to 49.44% when the amount of AMK (X_2) decreases from 60 to 20 %w/w. Similarly, at higher levels of X_1, Y decreases from 62.0% to 49.82% when X_2 increases from 20 to 60% w/w. The probable explanation for this may be change of bulk properties of ALLP due to L-leucine, producing ultra low density particles on spray drying, improves dispersibility of powders and act as flow aid (Lucas et al, 1999), whereas high proportion of TB/AMK may result dense particles, imparting poor dispersibility to ALLP.

It is evident from the Figures 4.10 to 4.13 that removal of L-leucine from the formulation greatly affect aerosol performance, poloxamer -188 at higher levels do not have significant effect on response Y and proportion of TB/AMK and poloxamer -188 at lower levels do not affect response Y. After achieving a polynomial equation and independent variables (X_1 to X_3) were optimized for the maximum response (Y). To verify the polynomial equation, ALLP were prepared according to the predicted levels of X_1, X_2, and X_3 and obtained response (Y) was found to non significantly ($P < 0.05$) different from the predicted value. The predicted and observed values are shown in Table 4.10. This demonstrated the reliability of the optimization procedure in predicting the aerosol performance of large respirable powders containing high therapeutic payload.

Table 4.8 Results of Each Experimental Run of TB-ALLP (Mean ± s.d., n=3).

Exp.No	VMD (μm)	Tap density g/cm^3	MMADt (μm)	Span	RMC (%)	EMC* (%)	ED (%)	MMADe (μm)
1	9.243 ± 0.314	0.046 ± 0.004	1.73 ± 0.082	1.325 ± 0.005	4.283 ± 0.177	1.235 ± 0.224	83.81 ± 1.605	2.01 ± 0.142
2	8.730 ± 0.126	0.054 ± 0.007	1.90 ±0.065	1.245 ± 0.018	4.068 ± 0.604	1.818 ± 0.166	83.52 ± 2.182	2.21 ± 0.204
3	6.856 ± 0.269	0.045 ± 0.005	1.62 ± 0.112	1.327 ± 0.042	4.846 ± 0.124	1.66 ± 0.238	88.60 ±2.956	1.71 ± 0.096
4	13.668 ± 0.176	0.052 ± 0.003	1.99 ± 0.078	1.572 ± 0.022	3.883 ±0.346	2.013 ± 0.270	87.15 ±3.05	2.63 ± 0.227
5	15.340 ± 0.583	0.041 ± 0.002	2.55 ± 0.172	1.769 ± 0.140	5.063 ± 0.556	1.483 ± 0.403	88.81 ± 2.242	2.81 ± 0.184
6	17.608 ± 0.221	0.048 ± 0.007	3.59 ± 0.191	1.956 ± 0.006	4.022 ± 0.524	1.742 ± 0.223	90.19 ± 1.341	2.08 ±0.118
7	11.491 ± 0.398	0.086 ±0.003	3.01 ± 0.184	2.315 ± 0.025	4.362 ± 0.373	1.910 ± 0.202	83.64 ± 2.054	3.28 ± 0.192
8	7.016 ± 0.316	0.044 ± 0.002	1.62 ± 0.194	1.635 ± 0.204	5.186 ± 0.695	1.586 ± 0.063	88.24 ±2.648	1.22 ± 0.092
9	9.652 ±0.244	0.042 ± 0.003	1.85 ± 0.079	1.687 ± 0.086	4.245 ± 0.466	1.682 ± 0.114	91.87 ± 2.146	2.45 ± 0.147
10	12.286 ±0.620	0.063 ± 0.005	3.17 ± 0.152	1.478 ± 0.007	3.906 ± 0.259	1.907 ±0.216	89.53 ± 3.022	3.43 ± 0.247
11	7.348 ±0.542	0.048 ± 0.002	1.83 ± 0.094	1.717 ±0.113	3.674 ± 1.02	2.182 ± 0.207	90.00 ± 1.926	1.62 ± 0.118
12	9.652 ± 1.120	0.071 ± 0.008	2.35 ± 0.087	1.684 ± 0.092	4.704 ± 0.724	1.854 ± 0.127	83.88 ± 2.212	2.75 ± 0.210
13	12.126 ± 0.809	0.074 ± 0.005	3.60 ± 0.107	1.758 ± 0.607	4.258 ± 0.634	1.425 ±0.312	83.87 ±1.554	2.98 ± 0.085
14	14.504 ± 0.423	0.057 ±0.004	3.74 ± 0.079	2.092 ± 0.086	5.106 ±1.106	2.089 ±0.561	90.15 ± 1.804	3.72 ± 0.314
15	13.870 ±0.762	0.047 ± 0.002	3.07 ± 0.117	1.775 ± 0.182	3.746 ± 0.892	1.523 ±1.112	84.98 ± 3.120	2.43 ± 0.115
16	11.085 ±0.658	0.042 ±0.006	1.81 ± 0.084	1.758 ± 0.158	5.074 ± 0.668	2.045 ±0.782	84.92 ± 2.413	2.06 ± 0.091

Table 4.9 Results of Each Experimental Run of AMK-ALLP (Mean ± s.d., n=3).

Exp.No	VMD (μm)	Tap density g/cm^3	MMADt (μm)	Span	RMC (%)	EMC* (%)	ED (%)	MMADe (μm)
1	8.247 ± 0.304	0.044 ± 0.001	1.98 ± 0.120	1.528 ± 0.159	3.883 ± 0.214	2.218 ± 0.11	78.90 ± 2.114	1.99 ± 0.096
2	8.030 ± 0.114	0.056 ± 0.004	2.02 ±0.084	1.436 ± 0.006	4.215 ± 0.527	1.664 ± 0.087	84.45 ± 1.096	2.24 ± 0.22
3	7.552 ± 0.165	0.046 ± 0.001	1.45 ± 0.212	1.376 ± 0.003	4.667 ± 0.097	1.754 ± 0.118	86.52 ±2.022	1.94 ± 0.147
4	9.084 ± 0.096	0.048 ± 0.003	3.11 ± 0.164	1.608 ± 0.018	4.283 ±0.228	1.944 ± 0.192	88.02 ±1.19	2.83 ± 0.327
5	12.440 ± 0.128	0.042 ± 0.003	3.10 ± 0.112	1.853 ± 0.240	4.073 ± 0.213	1.602 ± 0.313	91.54 ± 3.421	3.24 ± 0.245
6	16.748 ± 0.314	0.046 ± 0.005	2.51 ± 0.162	2.015 ± 0.030	4.412 ± 0.169	1.554 ± 0.447	91.65 ± 1.522	2.46 ±0.254
7	10.506 ± 0.314	0.082 ±0.002	3.36 ± 0.221	2.040 ± 0.027	3.967 ± 0.263	2.01 ± 0.117	82.95 ± 1.872	2.78 ± 0.274
8	7.616 ± 0.207	0.045 ± 0.007	1.47 ± 0.094	1.417 ± 0.124	4.892 ± 0.259	1.598 ± 0.073	89.11 ±3.212	1.57 ± 0.184
9	9.248 ±0.241	0.040 ± 0.001	1.97 ± 0.152	1.725 ± 0.112	5.016 ± 0.512	2.022 ± 0.067	92.25 ± 1.138	2.22 ± 0.115
10	13.064 ±0.476	0.059 ± 0.003	3.08 ± 0.109	1.519 ± 0.088	4.707 ± 0.439	1.945 ±0.146	87.84 ± 2.442	2.63 ± 0.321
11	8.116 ±0.642	0.051 ± 0.001	1.60 ± 0.192	1.686 ±0.213	5.166 ± 0.974	1.542 ± 0.148	92.04 ± 2.322	1.85 ± 0.084
12	8.652 ± 0.680	0.074 ± 0.004	2.57 ± 0.168	1.604 ± 0.085	4.854 ± 0.574	2.23 ± 0.254	85.74 ±3.16	1.85 ± 0.351
13	13.048 ± 0.742	0.076 ± 0.002	3.29 ± 0.104	1.912 ± 0.205	5.2.33 ± 1.116	1.587 ±0.222	86.62 ±2.332	3.01 ± 0.174
14	15.145 ± 0.337	0.061 ±0.003	3.46 ± 0.175	2.110 ± 0.108	4.284 ±1.224	1.350 ±0.246	90.44 ± 1.775	3.70 ± 0.227
15	14.644 ±0.664	0.044 ± 0.001	3.00 ± 0.213	1.873 ± 0.112	4.521 ± 0.562	1.655 ±0.652	83.96 ± 1.450	2.78 ± 0.245
16	9.068 ±0.452	0.040 ±0.006	2.27 ± 0.182	1.767 ± 0.201	4.587 ± 0.957	1.758 ±0.112	82.76 ± 3.225	2.36 ± 0.194

Table 4.10 Features of optimized ALLP (Mean ± s.d., n=3).

ALLP	Variable	Nominal value (%w/w)	Observed response value (Y;FPF)	Expected response value	VMD (μm)	Span	Tap density g/cm^3	MMADt (μm)	MMADe (μm)	GSD
TB-ALLP	X1	20.0	62.82 ± 2.86	64.708 ±7.17	6.712 ±0.314	1.237 ±0.003	0.044 ±0.006	1.40 ± 0.051	1.72 ± 0.097	1.448 ± .207
	X2	44.17								
	X3	1.19								
AMK-ALLP	X1	20.0	64.17 ± 3.13	71.21 ± 15.18	7.204 ±0.167	1.302 ±0.002	0.042 ±0.005	1.47 ± 0.032	1.69 ± 0.117	1.624 ±0.197
	X2	47.85								
	X3	1.0								

Morphological features (Mean ± s.d., n=10)

	Roundness	Elongation ratio	Fractal dimension	Heterogeneity	Clumpiness
TB-ALLP	1.048 ± 0.032	1.206 ± 0.164	1.036 ± 0.007	0.289 ± 0.067	0.045 ± 0.026
AMK-ALLP	1.064 ± 0.012	1.116 ± 0.094	1.028 ± 0.002	0..268 ± 0.064	0.046 ± 0.018

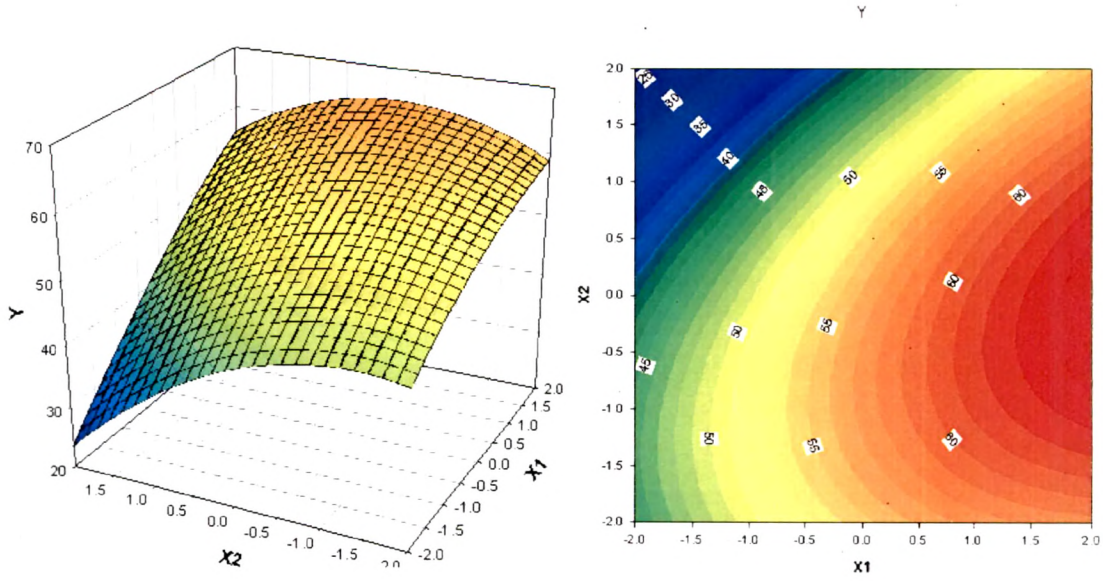

(A) (B)

Figure 4.8 **3D-Response surface plot (A) and Contour plot (B) showing the effect of the amount of L- leucine (X_1) and TB (X_2) added on the response Y (FPF).**

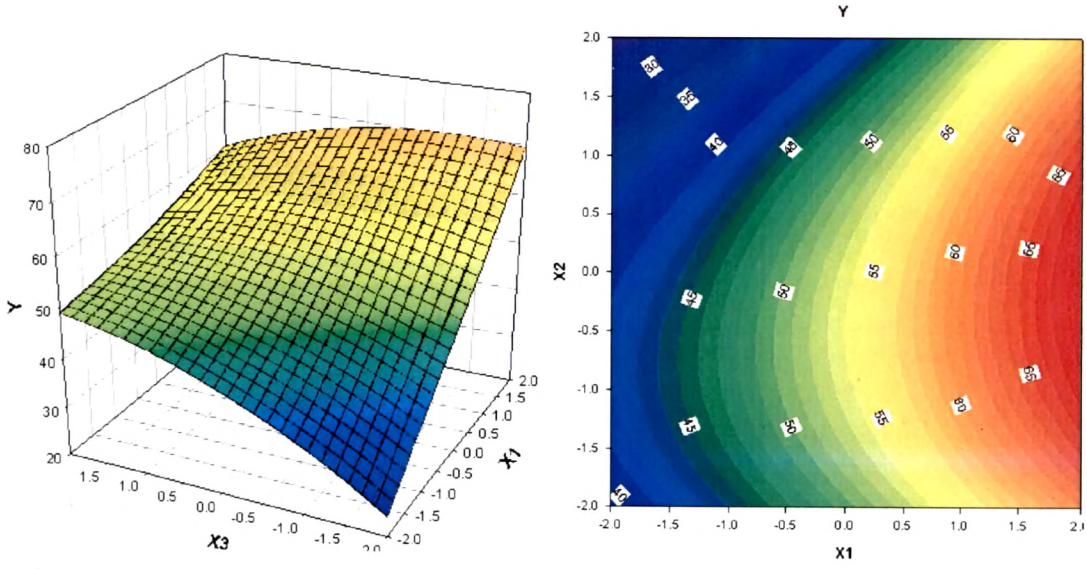

(A) (B)

Figure 4.9 **3D-Response surface plot (A) and Contour plot (B) showing the effect of the amount of L- leucine (X_1) and AMK (X_2) added on the response Y (FPF).**

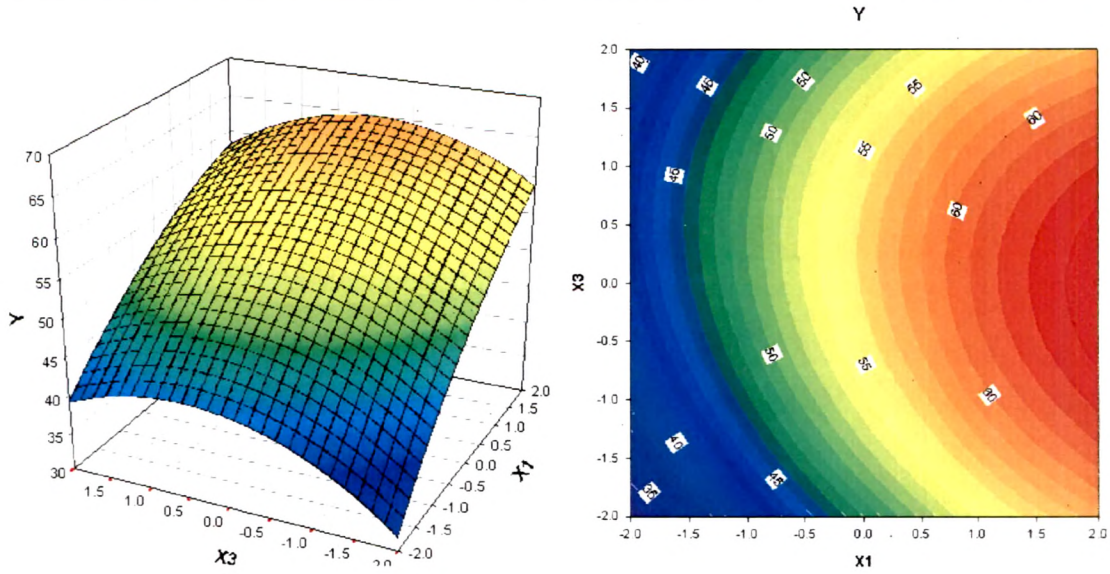

(A) (B)

Figure 4.10 **3D-Response surface plot (A) and Contour plot (B) showing the effect of the amount of L- leucine (X_1) and poloxamer- 188 (X_3) added on the response Y (FPF) of TB ALLP**

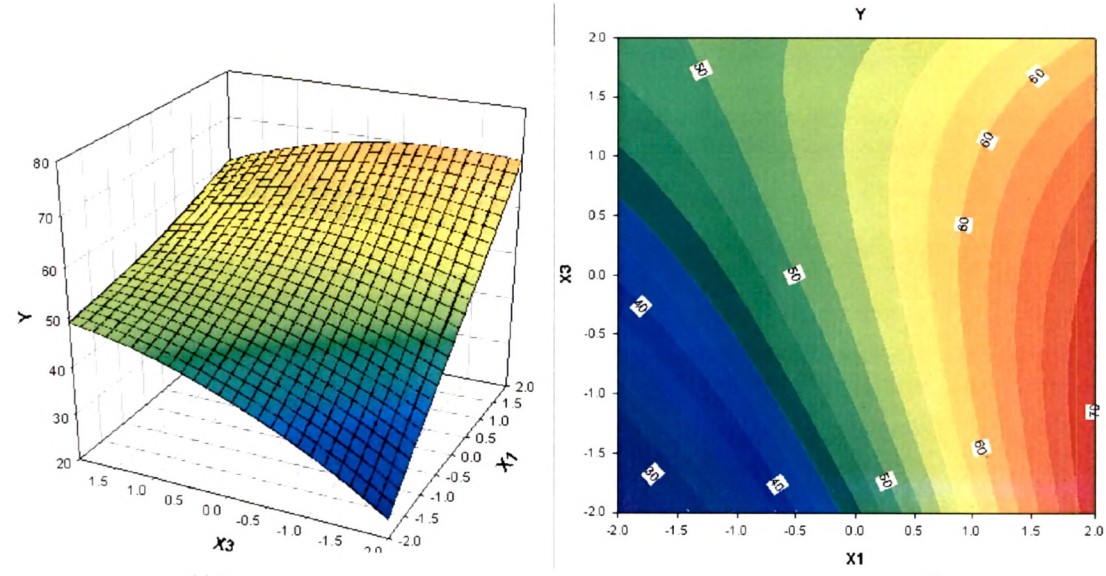

(A) (B)

Figure 4.11 **3D-Response surface plot (A) and Contour plot (B) showing the effect of the amount of L- leucine (X_1) and poloxamer- 188 (X_3) added on the response Y (FPF) of AMK ALLP**

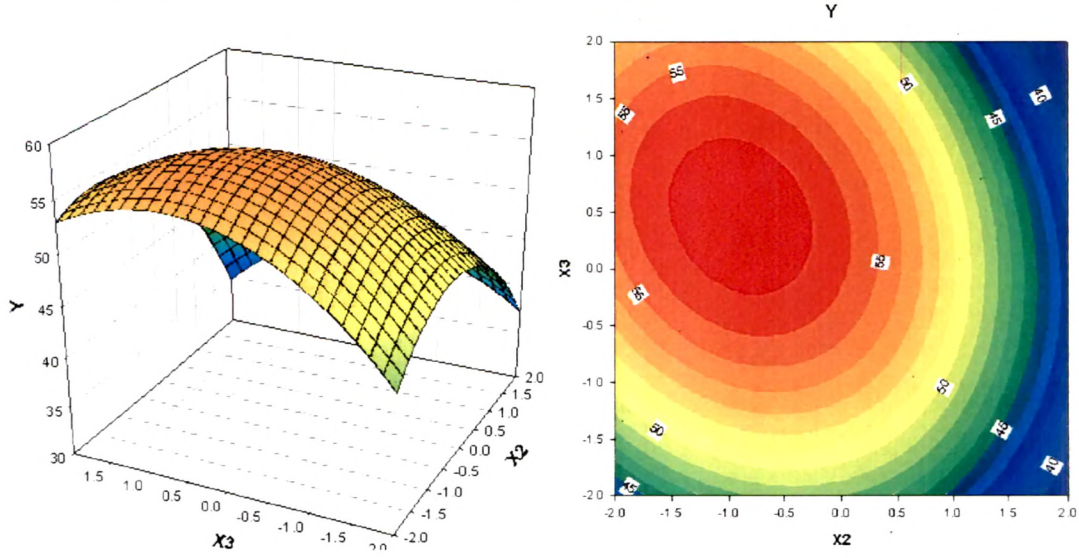

(A) (B)

Figure 4.12 **3D-Response surface plot (A) and Contour plot (B) showing the effect of the amount of TB (X2) and poloxamer- 188 (X_3) added on the response Y (FPF).**

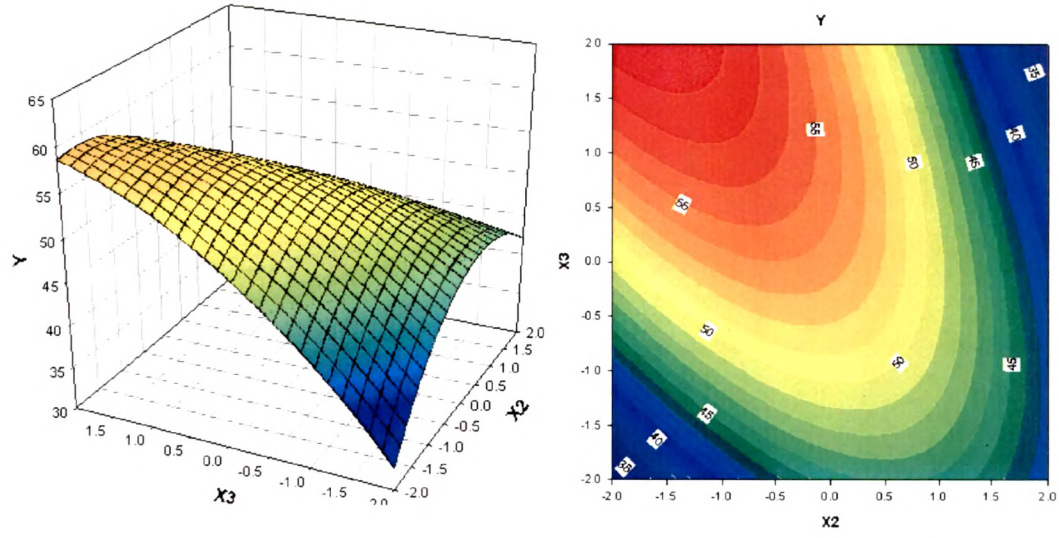

(A) (B)

Figure 4.13 **3D-Response surface plot (A) and Contour plot (B) showing the effect of the amount of AMK (X2) and poloxamer- 188 (X_3) added on the response Y (FPF).**

As shown in Table 4.11, ALLP produced by optimized values of formulation components presented a geometric particle size (VMD) of 6.712 μm ± 0.314 μm, 7.204±0.167; span of 1.237 ± 0.003, 1.302 ±0.002; tap density of 0.044 ±0.006, 0.042 ±0.005 g/cm^3 and MMADt of 1.40 ± 0.05 μm, 1.47 ± 0.032 for TB and AMK ALLP respectively. Morphological features further revealed that particles are nearly spherical in shape and having relatively smooth surface texture. Good reproducibility of the dry powder preparation was demonstrated by producing and characterizing powders made of optimized proportions of L-leucine/TB/poloxamer-188. The aerosolization properties of ALLP were evaluated with L-leucine/TB/poloxamer-188/HSPC formulations, keeping large mean particle size (greater then 6μm) and MMADt at 1-5 μm. The recoverable powder mass for all formulations were with in the range of 96.0 ± 2% of mass of powder filled into capsules, suggesting the method of washing and analyzing was accurate and reproducible. The fraction of all particles smaller than 5 μm represents the fine particle fraction (FPF<5 μm). The emitted doses in the Andersen cascade impactor operated at 28.3 L/min using a Rotahaler inhaler device was between 83-92 %,79-92%; FPF 40- 62 %, 37-66% and the MMADe of 1.22-3.27 μm and 1.57-3.70 μm for TB and AMK ALLP respectively. Proportion of formulation components greatly affected in vitro deposition. ALLP presenting similar density, geometric size and MMADt, were prepared with varying HSPC content. Amount of L-leucine and TB/AMK had significant effect ($P<0.05$) on in vitro deposition and FPF as high as 62.8±2.6% and 64.17±2.6% reached with the formulation L-leucine/TB/poloxamer-188/HSPC at 20/44.17/1.19/34.64 w/w/w/w and L-leucine/AMK/poloxamer-188/HSPC at 20/47.85/1.0/31.15 w/w/w/w respectively. ALLP containing a high drug (TB/AMK) load of 44.17 and 47.85 % w/w were prepared by spray drying technique using L-leucine/poloxamer- 188/HSPC. L-leucine was found to be most influencing component and increase in TB/AMK proportion above 50% w/w produced dense particles leading to poor aerosol performance. While, poloxamer-188 found to influence aerosol performance at low concentration (1-2 %w/w). The maximum fine particle fraction of 62.8 ±2.6% and 64.17±2.6% was obtained with L-leucine/TB/poloxamer-188/HSPC at 20/44.17/1.19/34.64 w/w/w/w and L-leucine/AMK/poloxamer-188/HSPC at 20/47.85/1.0/31.15 w/w/w/w of ALLP respectively. Particles were dimpled spherical shape with roundness value close to 1 and were having smooth surface texture with good powder dispersibility suitable for use in carrier-free dry powder inhalers. The above optimized ALLP formulations are selected for further evaluation of powder characteristics, stability studies and in-vivo studies.

4.7 REFERERENCES

Chew N.Y.K., and Chan H.-K. Effect of powder polydispersibility on aerosol generation. J.Phar. Pharm. Sci. 2002; 5(2): 162-168.

Chew N. Y. K., and Chan H.-K. Use of solid corrugated particles to enhance aerosol performance. Pharm. Res. 2001; 18:1570–1577.

Chew N.Y.K., Tang P., Chan H.–K., and Judy A. R. How much particle surface corrugation is sufficient to improve aerosol performance of powders? Pharm.Res. 2005; 22:148-152.

Hickey A.J., Martonen T.B., and Yang Y. Theoretical relationship of lung deposition to the fine particle fraction of inhalation aerosols. Pharm. Acta Helv. 1996; 71: 185–190.

Hickey A.J., Martonen T.B., and Yang Y. Theoretical relationship of lung deposition to the fine particle fraction of inhalation aerosols. Pharm. Acta Helv. 1996; 71: 185–190.

Larhrib H., Martin G.P., Prime D., and Marriott C. Characterisation and deposition studies of engineered lactose crystals with potential for use as a carrier for aerosolised salbutamol sulfate from dry powder inhalers. Eur. J. Pharm. Sci. 2003; 19: 211–221.

Lucas P., Anderson K., Potter U.J., and Staniforth J. N. Enhancement of small particle size dry powder aerosol formulations using ultra low density additive. Pharm. Res. 1999; 16 (10):1943-1647.

Monographs, Tobramycin sulfate. United States Pharmacopoeia 27, CD-ROM. 2004.

Monographs, Medicinal and Pharmaceutical substances, Amikacin sulfate sulfate. British Pharmacopoeia, CD-ROM. 2004.